**Repositorio Institucional de la Universidad Autónoma de Madrid**

https://repositorio.uam.es

Esta es la **versión de autor** del artículo publicado en:
This is an **author produced version** of a paper published in:

ACS Applied Materials and Interfaces 7.9 (2015): 5331-5337

DOI: http://dx.doi.org/10.1021/am508752m

**Copyright:** © 2015 American Chemical Society

El acceso a la versión del editor puede requerir la suscripción del recurso
Access to the published version may require subscription

# Effects of Hydroxylation and Silanization on the Surface Properties of ZnO Nanowires

*C. García Núñez,[†] M. Sachsenhauser,[‡] B. Blashcke,[‡] A. García Marín,[†] Jose A. Garrido[‡] and Jose L. Pau[†]*

[†] Grupo de Electrónica y Semiconductores, Departamento Física Aplicada, Universidad Autónoma de Madrid, C/ Francisco Tomás y Valiente 7, 28049 Madrid, España

[‡] Walter Schottky Institut and Physik-Department, Technische Universität Mün, Am Coulombwall 4, 85748 Garching, Germany

**Abstract**

Silanization is commonly used to form bonds between inorganic materials and biomolecules as a step in the surface preparation of solid-state biosensors. This work investigates the effects of silanization with amino-propyldiethoxymethylsilane (APDEMS) on hydroxylated sidewalls of zinc oxide (ZnO) nanowires (NWs). The surface properties and electrical characteristics of NWs are analyzed by different techniques after their hydroxylation and later silanization. Contact angle measurements reveal a stronger hydrophobic behaviour after silanization, and X-ray photoelectron spectroscopy results show a reduction of the surface dipole induced by the replacement of the hydroxyl group with the amine terminal group. The lower work function obtained after silanization in contact potential measurements corroborates the attenuation of the surface dipole observed in XPS. Furthermore, the surface band bending of NWs is determined from surface photovoltage measurements upon irradiation with UV light, yielding a 0.5 eV energy in hydroxylated NWs, and 0.18 eV, after silanization. From those results, a reduction in the surface state density of $3.1\times10^{11}$ $cm^{-2}$ is estimated after silanization. The current-voltage (*I-V*) characteristics measured in a silanized single NW device show a reduction of the resistance, due to the enhancement of the conductive volume inside the NW, which also improves the linearity of the *I-V* characteristic.

Keywords: ZnO nanowires; hydroxylation; silanization; surface band bending; contact potential difference; surface photovoltage; X-ray photoemission spectroscopy

## 1. Introduction

Nanowires (NWs) are outstanding materials for the development of gas and biological sensors due to their high surface-to-volume ratio. Beside their excellent optical and electrical properties, one of the advantages of zinc oxide (ZnO) material over other wide band gap semiconductors is the extensive variety of nanostructures (wires, belts, combs, springs, helixes, rings, cages,[1] tetrapods[2]…) that can be grown by cost-effective techniques such as vapor phase transport (VPT),[3] or solution-phase synthesis.[4] Particularly, ZnO based NWs have been thoroughly studied in the last years due to its facile fabrication procedure and suitable properties for the development of gas sensing[5,6] and UV light detection applications.[7,8] The axial electrical conduction of ZnO NWs is strongly influenced by the negative charges trapped in the sidewall surface and the consequent surface band bending (BB).[7] The adsorption of oxygen at the ZnO surface occurs by trapping free electrons from the NW bulk, thus reducing the electrical conductivity of the NW. Illumination of the NWs with UV light produces an excess of photo-generated holes that are swept to the surface and recombined through the surface levels turning them into neutral states. As a result of this process, oxygen is released from the surface while trapped negative charges are moved towards the NW core, resulting in a reduction of the space charge region (SCR) width ($w_{SCR}$) at the surface. After UV illumination, the recovery time is governed by the trapping times in the surface levels, leading to long reset times.[9,10]

The fabrication of biosensors requires the functionalization of the surface using self-assembled monolayers (SAM) to attach recognition elements such as antibodies, single-stranded DNA, or enzymes. The covalent binding of an organic SAM onto the ZnO surface has been demonstrated using carboxylic acid,[11,12] thiol[13,14] and silane[15,16] based compounds as linkers. However, most of those works are focused on the chemical modification of ZnO nanoparticles and films, with few studies addressing the surface functionalization of ZnO

NWs.[17] In this work, we study the silanization of ZnO NWs after surface hydroxylation by oxygen plasma. The silanization process of hydroxylated ZnO is based on the displacement of alkoxy groups in the silane molecule by the hydroxyl groups (-OH), forming Si-O-Si covalent bonds along the ZnO surface.[18] In general, the formation of the SAM is expected to induce changes in the electronic structure of the surface with different charge transfer phenomena that can affect the current-voltage (*I-V*) characteristics of the NWs and modify the electrical contact characteristics between NW and electrode.[19]

Contact potential difference (CPD) and surface photovoltage (SPV) measurements allow for non-destructive and contactless investigation of the surface energetics of metals and semiconductors. Whereas CPD measurements performed in dark allow quantification of the work function and surface charge density, SPV provides information about the surface BB. The exposure of the surface to sufficiently intense above-band gap light leads to the splitting of the quasi-Fermi levels, the screening of surface charges, and the flattening of the surface BB. Therefore, the variation of the CPD value under that kind of illumination provides a direct measurement of the surface BB.

In this work, the ZnO surfaces are analyzed by contact angle measurements, scanning electron microscopy (SEM), atomic force microscopy (AFM) and X-ray photoelectron spectroscopy (XPS) in order to characterize the surface properties after hydroxylation and silanization. In addition, the effect of the chemical modification on the surface BB is analyzed by CPD and SPV measurements. Finally, *I-V* characteristics in single ZnO NW devices are analyzed in dark conditions in order to study the effects of the BB variations on the electrical conduction of the NW. For this characterization, a single NW is aligned and integrated between a pair of conductive electrodes by means of dielectrophoresis (DEP).

## 2. Experimental details

## A. Material

Vertically aligned ZnO NWs are grown by chemical vapor transport using a Tempress quartz furnace as thoroughly explained elsewhere.[20] These NWs are synthesized on a Si(100) substrate covered with a 7-nm thick Zn seed layer, using micro-sized Zn powder (5.5 N purity) and $O_2$ as solid and gas precursors, respectively, and Ar as carrier gas. Described process is carried out at 900 ºC during 180 s, utilizing a mass of Zn powder of 0.5 g, an Ar:$O_2$ ratio of 1:1, and a total gas flux of 200 sccm, obtaining NWs with diameters between 100 and 500 nm and average lengths of 10 μm as determined by SEM. The resulting samples are analyzed by the techniques mentioned above. For the sake of comparison, a high purity a-plane ZnO bulk crystal, whose non-polar surface resembles the NW facet (m-plane),[21] is used as a reference sample in both contact angle and XPS measurements. In order to prepare a uniform dispersion of NWs for the processing of an electronic device, the NW sample is immersed in ethanol and sonicated for a few seconds. Further processing steps towards the fabrication of a single NW device are described in section G.

## B. Hydroxylation and silanization of ZnO surfaces

For the hydroxylation of m-plane (NW sidewall) and a-plane (bulk crystal) ZnO surfaces, both samples are sequentially dipped in hot ethanol, acetone and ethanol for 5 minutes, dried in $N_2$ and finally transferred to a oxygen plasma system (100-E TePla). Once the samples are loaded into the plasma chamber, it is pumped down to $10^{-1}$ mbar in order to preserve the chamber clean of contaminants; then, $O_2$ gas valve is opened, increasing the residual pressure up to 1.4 mbar. Finally, a 200-W power plasma is turned on for 5 minutes. Plasma treatment ensures the completely cleaning of surface organic contaminants and also promotes the formation of a uniform and stable coverage of -OH on the ZnO surface.[22] The silanization process is carried out in a glove box under Ar ambient ($O_2$ < 1 ppm and $H_2O$ < 2 ppm) in order to prevent the oligomerization of APDEMS molecules due to the ambient exposure.[23]

The samples are dipped in an APDEMS solution (0.02 M APDEMS in toluene) and stored in the glove box for 90 min. After that, samples are rinsed in toluene, isopropanol and dried in $N_2$.

### C. Static water contact angle measurements

A home-made system is used to investigate the contact angle of deionized water (resistivity, $\rho$ = 18 MΩ cm) droplets on the chemically modified m-plane and a-plane surfaces of NW and bulk reference samples, respectively. Images of 3 µl droplets deposited onto the sample surfaces are acquired using a video camera and later analyzed by image processing software with an accuracy of ±1º.

### D. Scanning electron microscopy and atomic force microscopy

The morphology of the sample surface is analyzed by SEM (Philips XL30) at 10 kV operation voltage, and AFM images obtained with a Digital Instruments MultiMode system in tapping-mode using silicon tips at scan frequencies between 0.5 and 0.8 Hz. Image processing, including analysis of step heights, surface roughness, and homogeneity are performed using Nanoscope and WSxM software.

### E. X-ray photoelectron spectroscopy

Surface chemical changes are analyzed by XPS, carried out in an ultrahigh vacuum system equipped with a SPECS XR-50 Mg-Anode X-ray source ($KE_\alpha$ = 1253.6 eV) and a SPECS Phoibos 100 hemispherical analyzer with an MCD-5 detector. Experimental data are acquired using a pass energy of 25 eV at a takeoff angle of 0° relative to the surface normal. The examined area is adjusted to about 7 $mm^2$ using a combination of a mechanical aperture, entrance and exit slits, and electron optics of the analyzer.

For analysis, the raw data are processed by subtraction of a linear or Shirley backgrounds and fitted with a Gaussian-Lorentzian mixed function, also called quasi-Voigt, using the software CasaXPS provided by SPECS GmbH (Berlin, Germany)..[24] For the analytical

estimation of the relative element molar fraction, first the background accounting for the secondary electrons is removed using a Shirley function, then element peak is fitted using a Gaussian-Lorentzian mixed function. The integral of the peak is divided by a relative sensitivity factor (R.S.F.) which is characteristic of each element. The R.S.F. for N 1s, C 1s, Zn 2p3/2 and O 1s are 0.42 and 0.25, 4.8 and 0.66, respectively.

### F. Conductive potential difference and surface photovoltage

CPD and SPV measurements presented in this work are obtained under ultrahigh vacuum using a Besocke Delta Phi Kelvin Probe S vibrating gold mesh electrode controlled by a Besocke Kelvin Control 07 unit from Besocke Delta Phi GmbH (Jülich, Germany). All the CPD voltages are referenced to the gold work function ($\Phi_{Au}$ = 4.7 eV). Illumination is provided by a low pressure Hg lamp (Benda, Germany).

### G. Single NW device fabrication

Single NW devices are fabricated by dielectrophoretic alignment through a pair of 100-nm thick Al-doped ZnO electrodes defined by photolithography and chemical etching on $SiO_2$(200 nm)/Si(100) substrates. While an alternating current (AC) signal with an amplitude of 15 V and a frequency of 100 kHz is supplied between coplanar electrodes, a 2 μl droplet extracted from the NW dispersion prepared in section A is drop-casted onto the electrodes covering the gap area. The electrodes are AC biased until the ethanol is completely evaporated (< 1 min). The induced alternating electric field leads to the formation of a dipole moment in the NWs, which are driven towards the high electric field region found at the electrode gap (positive DEP). DEP conditions (amplitude and frequency) have been optimized in previous works in order to improve the NW alignment efficiency.[25] After alignment, both NW ends are covered with 100-nm thick Al electrodes defined by photolithography and lift-off, aiming to ensure good ohmic characteristics of the NW contacts. The gap width between electrodes tries to match the length of the NW giving some

room to both sides of the NW to stand on AZO electrodes. Shorter distances may cause electrode short-circuiting during the Al electrode formation whereas a much larger distance may reduce the probability of holding both sides of the NW during DEP. For those reasons, the distance between the AZO electrodes is chosen to be 6 μm. As the average NW length is about 10 μm, those electrodes make possible the interelectrode bridge with a few microns NW length standing on each electrode.

Then, ZnO NW surface is firstly hydroxylated and later silanized as explained above. Finally, *I-V* characteristics of the resultant device are measured at every surface treatment step in dark conditions, aiming to observe variations produced by -OH and APDEMS surface coverages on the electrical conduction of the NW.

## 3. Results and discussions

### A. Surface wettability

A 3 μl droplet of deionized water is drop-casted on top of an a-plane ZnO bulk crystal reference sample and a ZnO NW template after hydroxylation and silanization, following the procedures described above. Figure 1(a,b) show contact angle images after hydroxylation, presenting values around 5º and 15º for the bulk crystal and the NW sample, respectively, and revealing strong hydrophilic behaviour, as observed in previous works.[26] After silanization (figure 1(c,d)), the surface turns hydrophobic exhibiting an increase of the contact angles up to 55º, in the a-plane bulk crystal, and 83º, in the NW sample. The contact angle obtained for silanized a-plane bulk crystal sample is close to that value measured in SiC surfaces functionalized by APDEMS.[24] In addition, the higher contact angle observed in the NW sample is associated to the nanostructured morphology of the surface, which according to the Cassie's model,[27] the droplets can stand on forming a high contact angle.

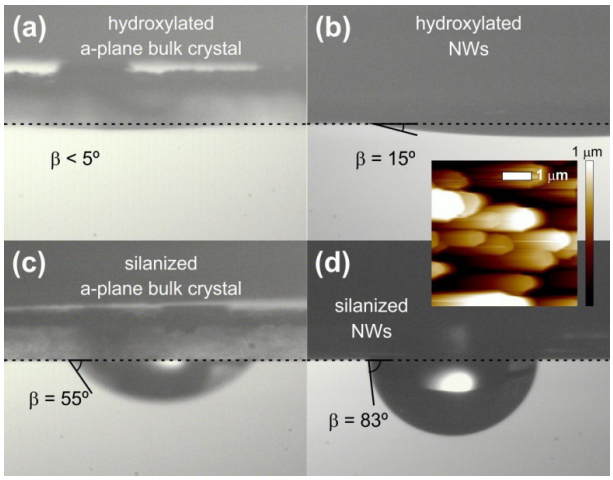


**Figure 1.** Contact angle measurements of a-plane ZnO bulk crystal and ZnO NW surfaces after (a,b) hydroxylation and (c,d) silanization. Inset, AFM image of vertically aligned ZnO NWs grown on a Si substrate.

### B. Surface chemical states

XPS spectra corresponding to N 1s, C 1s, Zn 2p3/2, and surface/bulk O 1s core levels measured in both a-plane ZnO bulk crystal and ZnO NWs samples after their hydroxylation and silanization. In comparison to the a-plane reference sample (not shown), it is worth noticing that the binding energies for all these elements in the NW sample are shifted about 3 eV towards larger values due to the geometry of the surface, which induces an extra stopping power when electrons from deeper atoms in the NW are photoemitted. Figure 2 shows XPS survey (a) and core levels (b-d) of ZnO NW sample after its hydroxylation (black) and silanization (red). First evidence of the silanization is the presence of a N peak (figure 2(b)), coming from the amine terminal group, and the increase of the C 1s peak (figure 2(c)), produced by the hydrocarbon groups in the APDEMS SAM. The origin of the C 1s signal in the hydroxylated sample is likely due to the unintentional C contamination of the ZnO bulk sample during the growth process.[20] After silanization, the C 1s peak increases and shifts 350 meV towards lower binding energies. These variations provide another evidence of the

presence of the SAM on the ZnO surface associated to the increase of the C molar fraction and the change in the chemical environment of the C atoms.

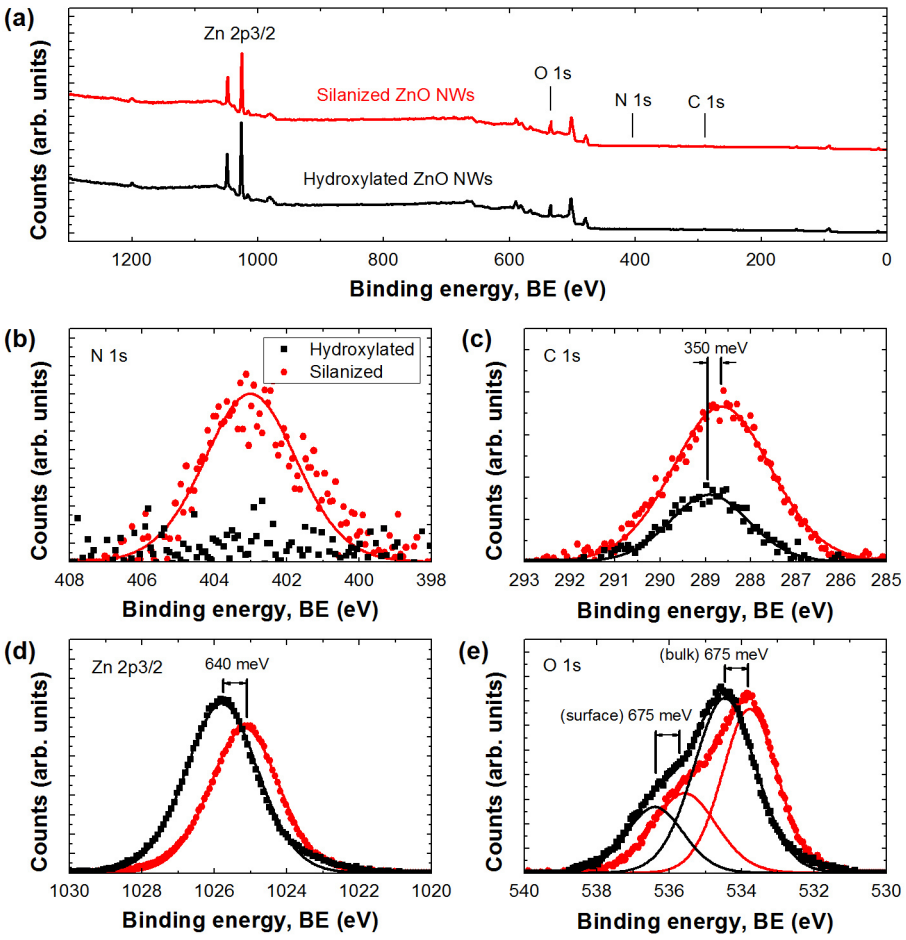


**Figure 2.** (a) XPS survey spectra of hydroxylated (black) and silanized (red) ZnO NW surfaces. (b) N 1s, (c) C 1s, (d) Zn 2p3/2 and (e) O 1s XPS core level spectra for ZnO NW surfaces after hydroxylation (black) and silanization (red). Solid lines represent the Gaussian-Lorentzian functions used to fit the signal of each element.

The attenuation of the Zn photoemission peak observed in figure 2(d) is another sign of the SAM formation atop the ZnO surface. Such attenuation can be used to determine the surface coverage and the SAM thickness ($d_{SAM}$) following the expression (1):[28]

$$d_{\mathrm{SAM}} = -\lambda_{\mathrm{n}} \ln\left(\frac{I_{\mathrm{SAM}}}{I_0}\right), \qquad (1)$$

where $\lambda_{\mathrm{n}}$ is the photon wavelength at the center of the peak, and $I_0$ and $I_{\mathrm{SAM}}$ are the photoelectron intensity after hydroxylation and silanization, respectively. Expression (1) is used to determine the $d_{\mathrm{SAM}}$ in the NW and a-plane bulk crystal samples yielding values of 0.37 and 0.58 nm, respectively. Surface coverage is calculated from those values, using expression (2):

$$\Gamma(\mathrm{molecules/cm^2}) = \frac{d_{\mathrm{SAM}}\ \rho_{\mathrm{APDEMS}}\ N_{\mathrm{A}}}{M_{\mathrm{APDEMS}}}, \qquad (2)$$

where $\rho_{\mathrm{APDEMS}}$ and $M_{\mathrm{APDEMS}}$ are the density and molar mass of APDEMS, respectively, and $N_{\mathrm{A}}$ is the Avogadro's constant. From expression (2), the surface coverage after silanization is calculated to be $8.0\times10^{13}$ molecules/cm$^2$ in the NW sample and $12.6\times10^{13}$ molecules/cm$^2$ in the a-plane bulk crystal sample. Comparing to the total achievable surface coverage for an a-plane ZnO surface ($6.82\times10^{14}$ molecules/cm$^2$), the resultant surface concentrations correspond to coverages of 11.7% and 18.5%, respectively.

After using the R.S.F. given in section 2E in Zn (figure 2(d)) and O bulk (figure 2(e)) signals, the O(bulk):Zn ratio calculated for the non-silanized sample is 1.03 confirming the stoichiometric characteristics of the NWs. After silanization, this factor remains near 1, suggesting that there are no significant changes in the atomic distribution of the bulk caused by the SAM formation.

Figure 2(e) shows the surface and the bulk O peaks for the NW sample after its hydroxylation and silanization. We have first focused on the variation of the surface O. The integral to the Gaussian-Lorentzian fit under the surface O peak is calculated and corrected

by both the R.S.F. and the molar factors. For the hydroxylated surface, it must be taken into account that -OH groups bind to the Zn atom under a stoichiometric ratio of 2:1 to form $Zn(OH)_2$ (figure 3(a)); therefore, the molar factor is 2. In contrast, silanized samples have APDEMS molecules attached to the ZnO surface (figure 3(b)), resulting in a stoichiometry ratio of Zn:O=1:3 and yielding an effective molar factor of 3. The ratio between the surface O signals in silanized and hydroxylated samples results in 0.9; using this ratio and the surface coverage calculated for APDEMS ($8.0\times10^{13}$ molecules/$cm^2$), the surface coverage of hydroxylated NWs is expected to be around $8.9\times10^{13}$ molecules/$cm^2$. This result points out the efficiency of the initial -OH coverage to promote the attachment of the APDEMS molecules, indicating that most of the -OH groups should be nearly replaced by APDEMS molecules along the ZnO surface.

The successful formation of the SAM on the ZnO surface can be also demonstrated by analyzing the energy shift of the XPS peaks. Figure 2(d) presents a strong energy shift (640 meV) of the Zn peak towards lower binding energies after the silanization step. This can be attributed to the attenuation of the negative surface dipole, formed after hydroxylation (figure 3(a)), by the charges in the APDEMS molecules (figure 3(b)). In the hydroxylated samples, the kinetic energy of the photoemitted electrons from the ZnO bulk is reduced due to the influence of the negative surface dipole. Finally, the evidence of the presence of a surface dipole change is also observed in both the O bulk and surface signals which present a binding energy shift of approximately 675 meV toward lower binding energies (figure 2(e)).

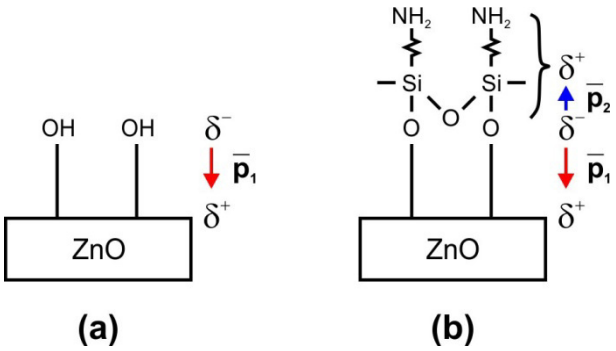


**Figure 3.** ZnO surface dipoles formed after (a) hydroxylation and (b) silanization.

### C. Surface band bending

CPD measurements are taken in order to find out changes in the surface work function of the NW sample due to the formation of the different surface dipoles after hydroxylation or silanization. Those dipoles can affect the surface BB of the energy bands, which determines the $w_{SCR}$ and the transverse conduction volume along the NW.

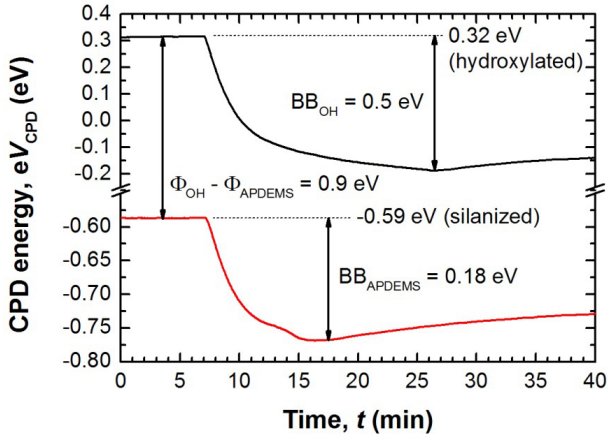


**Figure 4.** CPD and SPV voltages measured for hydroxylated (red) and silanized (black) ZnO NW samples.

Following the hydroxylation treatment, ZnO NW samples exhibited a dark CPD value of $eV_{CPD}$ = +0.32 eV (CPD energy plateau observed in the black curve of figure 4 for times

ranged between 0 and 7 min), which corresponds to the voltage necessary to nullify the difference between the Au work function ($\Phi_{Au}$ = 4.7 eV) and the surface work function ($\Phi$), defined as the sum of the ZnO work function ($\Phi_{ZnO}$), the surface BB ($\Phi_s$) and the energy step associated to the negative surface dipole induced by the hydroxyl group ($\Phi_{OH}$) (figure 5(a)). Therefore, the surface work function of the hydroxylated ZnO NW surface is estimated to be $\Phi = eV_{CPD} + \Phi_{Au}$ = 5.02 eV.

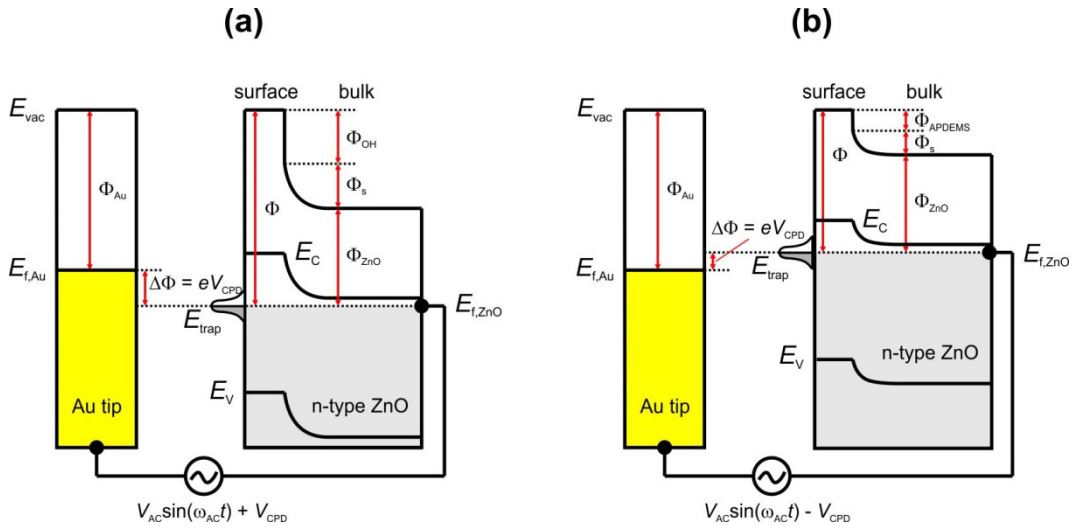


**Figure 5.** Electronic band structure of (a) hydroxylated and (b) silanized ZnO NW surface for CPD measurements.

For silanized surfaces, the dark CPD values decreases down to -0.59 eV (CPD energy plateau observed in the red curve of figure 4 for times ranged between 0 and 7 min), which means that the local vacuum level is lowered by a negative energy step induced by the reduction of the surface dipole, due to the charge distribution in the adlayer $\Phi_{APDEMS}$ (figure 5(b)). Then, the surface work function of the silanized ZnO NW surface is calculated to be $\Phi = eV_{CPD} + \Phi_{Au}$ = 4.11 eV. As $V_{CPD}$ is negative in this case, the work function of the silanized

surface is lower than the Au work function. This is a direct consequence of surface dipole reduction after silanization also observed in the XPS analysis of the O peak.[24]

During the SPV measurements, the use of a strong illumination above the band gap energy of ZnO produces BB flattening in hydroxylated and silanized samples which allows determining $\Phi_s$. The $\Phi_s$ value obtained for hydroxylated and silanized ZnO NW surfaces are found to be 0.5 and 0.18 eV, respectively. Using SPV ($\Phi_s$), CPD results ($\Phi$) and the ZnO work function reported in the literature for as-deposited ZnO ($\Phi_{ZnO}$ = 3.74 eV),[29] one can determine the surface dipoles $\Phi_{OH}$ and $\Phi_{APDEMS}$, resulting in 0.78 and 0.19 eV, respectively, being in good agreement with XPS results.

Solving the Poisson's equation, in thermal equilibrium, for a n-type semiconductor with a single set of discrete surface states of acceptor type, it is possible to obtain the density of surface states ($N_{ss}$) from the $\Phi_s$ expression (3):[30]

$$\Phi_s = \frac{(e\,N_{ss})^2}{2\,\varepsilon_{ZnO}\,\varepsilon_0\,N_d}, \qquad (3)$$

where $N_d$ is the donor density, $\varepsilon_{ZnO}$ is the relative permittivity for ZnO ($11\varepsilon_0$), $\varepsilon_0$ is the vacuum permittivity ($8.85\times10^{-12}$ C/V m), and $e$ is the electron charge ($1.602\times10^{-19}$ C). Assuming a $N_d$ of $10^{17}$ $cm^{-3}$ **for VPT ZnO NWs,[31,32]** the $N_{ss}$ can be estimated for hydroxylated and silanized samples using expression (3) and obtained $\Phi_s$ values from CPD and SPV measurements (called $BB_{OH}$ and $BB_{APDEMS}$ in figure 4), resulting$7.8\times10^{11}$ and $4.7\times10^{11}$ $cm^{-2}$, respectively. Therefore, the decrease of the BB obtained after silanization is the result of a reduction in $N_{ss}$ of around $3.1\times10^{11}$ $cm^{-2}$ upon attachment of the organic adlayer.

**D. Single NW device characterization**

The surface studies discussed above are completed with the characterization of the electrical conductivity in a single ZnO NW. As the device fabrication method always ends up with an organic cleaning to remove the rests of photoresist after the lift-off stage, the described hydroxylation process stabilizes the surface providing a uniform and stable –OH group coating that helps the interpretation of the *I-V* results, setting a reproducible scenario for any further surface modification. Figure 6 shows a layer schematic and a SEM image of the resultant device. In the SEM image (figure 6(b)), dashed lines are used to highlight electrodes composed by Al and **Al doped ZnO** (AZO).

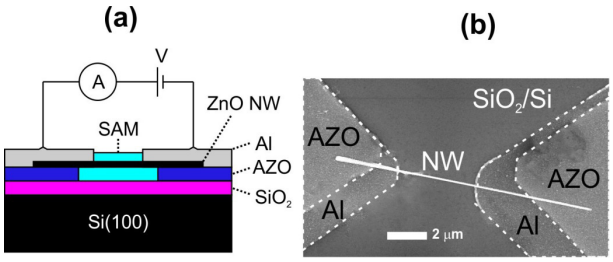


**Figure 6.** (a) Layer structure schematic and (b) SEM image of the single NW device.

*I-V* characteristics of the fabricated devices are measured after every surface treatment (figure 7). After hydroxylation (black curve), the device presents a current of 0.3 nA at 5 V which is much lower than those values measured in the NW devices before any surface treatment (blue curve) and a non-linear behaviour that will be analyzed in depth later on.

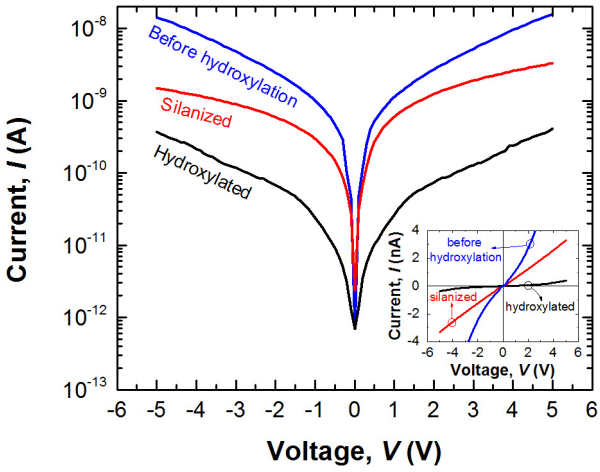


**Figure 7.** *I-V* characteristics of a single NW measured before (blue) and after hydroxylation (black) and silanization (red). Inset: *I-V* curves in linear scale.

Comparing to the hydroxylated device, the silanized device (red curve) presents higher current levels (3 nA at 5V). In order to understand this change of the current, the $w_{SCR}$ value is calculated at every step from the BB magnitude obtained in SPV measurements (figure 4) and using expression (4):[22]

$$\Phi_s = \frac{e^2}{2\varepsilon_{ZnO}\varepsilon_0} N_d w_{SCR} \quad . \qquad (4)$$

The values obtained for $w_{SCR}$ are 78 and 47 nm for hydroxylated and silanized devices, respectively. From figure 6(b), the NW radius ($r_{NW}$) and length are estimated to be around 60 nm and 4 μm, respectively. Subtracting $w_{SCR}$ from $r_{NW}$, the hydroxylated device is expected to be fully depleted ($w_{SCR} > r_{NW}$), while the silanized device has a $w_{SCR}$ value lower than the radius. Similar results have been obtained in a previous work, where current levels of devices with the same geometry were demonstrated to be directly related by $r_{NW}$ of the ZnO NW.[25] Therefore, that higher current levels measured in the silanized device (or even higher

untreated ZnO NW based devices) are suggested to be a direct consequence of the SCR narrowing, which means an increase of the conductive volume.

Furthermore, the increase of the conductive volume is also suggested to have a positive effect on the contact linearly such as observed in the inset of figure 7, where the *I-V* curve changes from non-linear to linear after silanization. Although the free charge emission mainly occurs from the naked surface of the NW, the increase of the free charge density inside the NW can enhance tunneling transport through the contact built-in voltage.[33] Quantum theory predicts that the increase of the carrier population in the NW increases the transmission probability through a potential barrier. This result agrees with a previous studies on NWs of different diameters,[25] where it is found that the increase of the conductive volume provokes, not only the increase of the conductivity, but also the improvement of the linearity of the *I-V* characteristic. Therefore, devices based on a single NW show non-linear *I-V* curves for nearly depleted NWs in contrast to devices with larger diameters and non-depleted volumes. From the results of the present work, it seems that the increase of the free charge inside the volume of a nearly-depleted NW through the passivation of surface states can also provoke the improvement of the contact linearity.

## Conclusions

ZnO NWs have been successfully functionalized with APDEMS as demonstrated by different techniques such as contact angle measurements, CPD, SPV and XPS. Silanization make the surfaces hydrophobic in comparison to the hydrophilic properties shown in the hydroxylated surfaces. The XPS spectra confirmed the attachment of the APDEMS molecules through the presence of N 1s and C 1s peaks, belonging to amine and hydrocarbon groups. The spectra also show a binding energy redshift (320 meV) of both peaks Zn 2p3/2 and O 1s comparing to the hydroxylated ZnO, evidencing a change in the surface dipole

formed atop the ZnO surface. This change of the surface dipole also produces a reduction of the ZnO work function from 5.02 eV (hydroxylation) to 4.11 eV (silanization) as determined by CPD. On the other hand, comparing the width of the surface BB obtained from SPV measurements with the NW axial dimensions, it can be concluded that the hydroxylated NWs are nearly depleted. The *I-V* characteristics of a single NW are measured integrating the NW between a pair of Al electrodes using dielectrophoresis. The silanized NW shows larger currents than the hydroxylated NW due to the enlargement of the conductive volume. Finally, it is observed that the NW silanization improves the linear characteristic of the contact formed between the NW and the Al electrode mainly due to the increase of the total free charge in the NW, which can benefit the output parameters of ion-gated field-effect transistors.

**Acknowledgements**

This work was partially carried out at the Walter Schottky Institute (Munich, Germany) and the Universidad Autónoma de Madrid (Madrid, Spain), and is partially supported by the Comunidad de Madrid R&D S2009/PPQ-1642, as well as the Spanish Ministry of Economy and Competitivity (MINECO) under TEC2010-20796, projects, which are gratefully acknowledged.

## Table of content (TOC) graphic

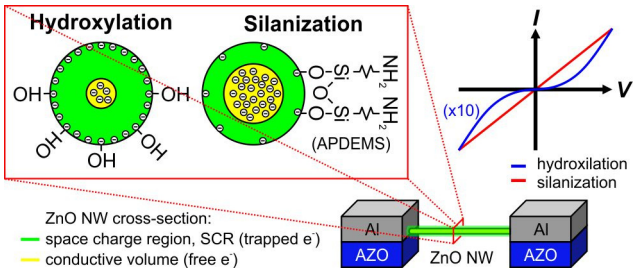

**References**

(1) Wang, Z.L. Zinc Oxide Nanostructures: Growth, Properties and Applications, *J. Phys.: Condens. Matter*. 2004, 16, R829−R858.

(2) Chen, Z. Zinc Oxide Nanotetrapods. *Nanotechnology* 2004, 15, 365−369.

(3) Huang, M. H. Catalytic Growth of Zinc Oxide Nanowires by Vapor Transport. *Adv. Mater*. 2001, 13,113−116.

(4) Greene, L. E.; Yuhas, B. D.; Law, M.; Zitoun, D.; Yang, P. Solution-Grown Zinc Oxide Nanowires. *Inorg. Chem.* 2006, 45, 7535−7543.

(5) Sberveglieri, G.; Baratto, C.; Comini, E.; Faglia, G.; Ferroni, M.; Ponzoni A.; Vomiero, A. Synthesis and Characterization of Semiconducting Nanowires for Gas Sensing. *Sens. Actuators B* 2007, 121, 208−213.

(6) Joshi, R. K. Au Decorated Zinc Oxide Nanowires for CO Sensing. *J. Phys. Chem. C* 2009, 113, 16199−16202.

(7) Soci, C.; Zhang, A.; Xiang, B.; Dayeh, S. A.; Aplin, D. P. R.; Park, J.; Bao, X. Y.; Lo, Y. H.; Wang, D. ZnO Nanowire UV Photodetectors with High Internal Gain. *Nano Lett.*, 2007, 7, 1003−1009.

(8) Suehiro, J.; Nakagawa, N.; Hidaka, S.; Ueda, M.; Imasaka, K.; Higashihata, M.; Okada, T.; Hara, M. Dielectrophoretic Fabrication and Characterization of a ZnO Nanowire-based UV Photosensor. *Nanotechnology* 2006, 17, 2567−2573.

(9) Liu, K.; Sakurai, M.; Liao, M.; Aono M. Giant Improvement of the Performance of ZnO Nanowire Photodetectors by Au Nanoparticles. *J. Phys. Chem. C* 2010, 114, 19835−19839.

(10) Seong, H.; Yun, J.; Jun, H.; Cho, K.; Kim, S. The Transfer of Charge Carriers Photogenerated in ZnO Nanoparticles into a Single ZnO Nanowire. *Nanotechnology* 2009, 20, 245201.

(11) Taratula, O.; Galoppini, E.; Wang, D.; Chu, D.; Zhang, Z.; Chen, H.; Saraf, G.; Lu, Y. Binding Studies of Molecular Linkers to ZnO Nanotips. *J. Phys. Chem. B* 2006, 110, 6506−6515.

(12) Taratula, O.; Galoppini, E.; Mendelsohn, R.; Reyes, P.; Zhang, Z.; Duan, Z.; Zhong, J.; Lu, Y. Stepwise Functionalization of ZnO Nanotips with DNA. *Langmuir* 2009, 25, 2107−2013.

(13) Sadik, P. W.; Pearton, S. J.; Norton, D. P.; Lambers, E.; Ren, F. Functionalizing Zn- and O-terminated ZnO with Thiols. *J. Appl. Phys.* 2007, 101, 104514.

(14) Deng, S. Z.; Fan, H. M.; Wang, M.; Zheng, M. R.; Yi, J. B.; Wu, R. Q.; Tan, H. R.; Sow, C. H.; Ding, J.; Feng, Y. P.; Loh K. P. Thiol-Capped ZnO Nanowire/Nanotube Arrays with Tunable Magnetic Properties at Room Temperature. *ACS Nano* 2010, 4, 495–505.

(15) Zeng, T. W.; Liu, I. S.; Huan, K. T.; Liao, H. C.; Chien, C. T.; Wong, D. K. P.; Chen, C. W.; Wu, J. J.; Chen, Y. F.; Su, W. F. Effects of Bifunctional Linker on the Optical properties of ZnO Nanocolumn-linker-CdSe Quantum Dots Heterostructure. *J. Colloid Interface Sci.* 2011, 358, 323−328.

(16) Niepelt, R.; Schröder, U. C.; Sommerfeld, J.; Slowik, I.; Rudolph, B.; Möller, R.; Seise, B.; Csaki, A.; Fritzsche, W.; Ronning C. Biofunctionalization of Zinc Oxide Nanowires for DNA Sensory Applications. *Nanoscale Res. Lett.* 2011, 6, 511.

(17) Pauporte, T.; Lincot, D. Electrodeposition of Semiconductors for Optoelectronic Devices: Results on Zinc Oxide. *Electrochim. Acta* 2000, 45, 3345−3353.

(18) Allen, C. G., Baker, D.J.; Albin, J. M.; Oertli, H. E.; Gillaspie, D. T.; Olson, D. C., Furtak, T. E.; Collins, R. T. Surface Modification of ZnO using Triethoxysilane-based Molecules. *Langmuir* 2008, 24, 13393−13398.

(19) Kim, S.; Carpenter, P. D., Jean, R.K.; Chen, H.; Zhou, C.; Ju, S.; Janes, D. B. Role of Self-assembled Monolayer Passivation in Electrical Transport Properties and Flicker Noise of Nanowire Transistors. *ACS Nano* 2012, 6, 7352−61.

(20) García Núñez, C.; Pau, J. L.; Ruíz, E.; García Marín, A.; García, B. J.; Piqueras, J.; Shen, G.; Wilbert, D. S.; Kim S. M.; Kung, P. Enhanced Fabrication Process of Zinc Oxide Nanowires for Optoelectronics. *Thin Solid Films* 2014, 555, 42−47.

(21) Wang, Z. L. Zinc Oxide Nanostructures: Growth, Properties and Applications. *J. Phys.: Condens. Matter*. 2004, 16, R829−R858.

(22) Woll, C. The Chemistry and Physics of Zinc Oxide Surfaces. *Prog. Surf. Sci.* 2007, 82, 55−120.

(23) Saddow, S. E. *Silicon Carbide Biotechnology*, 1st ed; Elsevier, 2012.

(24) Schoell, S. J.; Sachsenhauser, M.; Oliveros, A.; Howgate, J.; Stutzmann, M.; Brandt, M. S.; Frewin, C. L.; Saddow, S. E.; Sharp, I. D. Organic Functionalization of 3C-SiC Surfaces. *ACS Appl. Mater. Interfaces* 2013, 5, 1393−1399.

(25) García Núñez, C.; García Marín, A.; Nanterne, P.; Piqueras, J.; Kung P.; Pau, J. L. Conducting Properties of Nearly Depleted ZnO Nanowire UV Sensors Fabricated by Dielectrophoresis. *Nanotechnology* 2013, 24, 415702.

(26) Meng, X. Q.; Zhao, D. X.; Zhang, J. Y.; Shen, D. Z.; Lu, Y. M.; Dong, L.; Xiao, Z. Y.; Liu, Y. C.; Fan, X. W. Wettability Conversion on ZnO Nanowire Arrays Surface Modified by Oxygen Plasma Treatment and Annealing. *Chem. Phys. Lett.* 2005, 413, 450−453.

(27) Cassie, A. B. D.; Baxter, S. Wettability of porous surfaces. *Trans. Faraday Soc.* 1944, 40, 546−551.

(28) Johansson, E.; Nyborg, L. XPS Study of Carboxylic Acid Layers on Oxidized Metals with Reference to Particulate Materials. *Surf. Interface. Anal.* 2003, 35, 375−381.

(29) Kuo, F. L.; Li, Y.; Solomon, M.; Du J.; Shepherd, N. D. Work Function Tuning of Zinc Oxide Films by Argon Sputtering and Oxygen Plasma: an Experimental and Computational Study. *J. Phys. D: Appl. Phys.* 2012, 45, 065301.

(30) Mönch, W. *Semiconductor Surfaces and Interfaces*, 3rd ed; Springer: New York, 2001.

(31) Li, Q. H.; Liang, Y. X.; Wan, Q.; Wang, T. H. Oxygen Sensing Characteristics of Individual ZnO Nanowire Transistors. *Appl. Phys. Lett.* 2004, 85, 6389−6391.

(32) Chang, P. C.; Fan, Z.; Wang, D.; Tseng, W. Y.; Chiou, W. A.; Hong, J.; Lu, J. G. ZnO Nanowires Synthesized by Vapor Trapping CVD Method. *Chem. Mater.* 2004, 16, 5133−5137.

(33) Sze, S. M. *Physics of Semiconductor Devices*, 2nd ed; Wiley: New York, 1981.